ELSEVIER

Journal of Power Sources 73 (1998) 182–192

JOURNAL OF POWER SOURCES

Three-dimensional simulation of a molten carbonate fuel cell stack under transient conditions

W. He [a,*], Q. Chen [b,1]

[a] *Delft University of Technology, Faculty of Mechanical Engineering and Marine Technology, 2628 CD Delft, Netherlands*
[b] *Massachusetts Institute of Technology, Department of Architecture, Cambridge, MA 02139, USA*

Received 31 October 1997; accepted 10 November 1997

Abstract

A numerical model has been developed to simulate the parameters distribution in molten carbonate fuel cell (MCFC) stacks under transient conditions. The stack model is the extension of the cell model by taking account of the heat transfer and gas transport processes with regard to the stack configuration. The stack model has been implemented by using a computational-fluid-dynamics (CFD) program. This paper demonstrates the model performance by applying it to calculate the responses of current density and temperature distributions to a step voltage change. The simulated temperature profiles are consistent with the simulated and experimental results from the literature.

Keywords: Molten carbonate fuel cell stack; Three-dimensional simulation; Transient conditions

1. Introduction

The distributions of the crucial parameters (e.g., temperature and current density) in a molten carbonate fuel cell (MCFC) stack have a major impact on its safe and efficient operation. A commercially realistic MCFC stack has cells with a reaction area of about 1 m^2, and the temperature difference in the stack can be several hundred degrees Kelvin at maximum load [1]. When evaluating stack performance, it is important to accurately predict the stack temperature distribution because the local current density depends on the temperature. The stack temperature distribution also provides a basis for the stack engineering studies, such as the differential expansion, cell component corrosion and electrolyte evaporation losses due to large temperature gradients or high local cell temperature. In addition, the output power from an MCFC stack is directly used to follow the variation of consumer loads, possibly in conjunction with the electricity grid, therefore, the stack characteristics under transient conditions should also be identified. The experimental investigation of the distributions of the crucial parameters in a stack is expensive and can only be carried out on a small scale for a few designs, and moreover, measurement of the distributions, especially under transient conditions, is difficult. For these reasons, it is desirable to investigate an MCFC stack using numerical models.

The physical and chemical phenomena related to an MCFC stack load-following performance are considered at electrode, cell, and stack levels. A stack model therefore involves dealing with the processes at electrode, cell, and stack levels. The related literature information is as follows: (a) at electrode level, several models [2–4] have often been used to predict the local dependence of current density on electrodes structure and local operation conditions (e.g., temperature, pressure and gas composition). (b) At cell level, frequent reference is made to the cell model of Wolf and Wilemski [1]. This deals with cell processes in two-dimensional, steady-state form. The cell model takes account of gas stream utilization due to electrochemical reaction, conductive heat transfer between cell hardware and gas streams, energy transfer accompanying mass addition to the bulk streams, convective heat transfer by the bulk streams, and the heat conduction through the cell hardware. Individual porous electrode models are used to

* Corresponding author. Tel.: +31-15-2786978; fax: +31-15-2782460; e-mail: w.he@wbmt.tudelft.nl.
[1] Also corresponding author. Tel.: +1-617-253-7714; fax: +1-617-253-6152; e-mail: qchen@mit.edu.

0378-7753/98/$19.00

predict the local dependence of current density on cell temperature and gas composition. Watanabe et al. [4] extended the cell model of Wolf and Wilemski [1] to transient conditions, and proposed a new form of empirical correlation equation between the local cell performance and the operation conditions. (c) At stack level, Fujimura et al. [5] provided a three-dimensional, steady-state temperature distribution across a stack without reforming, which takes into account of the heat transfer in the stacking direction and between the end plates and the surroundings. Shinoki et al. [6] also provided a steady-state model for a stack with internal reforming. In addition, there are simplified one-dimensional or lumped stack models for integration into the system models [7–9]. These models do not provide the parameter distributions across a stack.

Among the fields of modeling fuel cells, such as the solid oxide fuel cell (SOFC), the phosphoric acid fuel cell (PAFC) and the proton exchange membrane (PEM) fuel cell, the SOFC activities are most relevant to our MCFC simulation. Achenbach [10,11] provided the current and temperature distributions in an SOFC stack under both steady-state and transient conditions. However, his model is still based on the assumption of a uniform gas distribution along the stack direction.

The above literature provides no indication that MCFC stack models are available for computing parameter distributions under transient conditions. This MCFC stack model is the extension of the cell model [4], taking account of the heat transfer [5] and gas transport processes with regard to the stack configuration under transient conditions. The implementation of the stack model uses a computational-fluid-dynamics (CFD) program PHOENICS [12], which is capable of dealing with the interconnected fluid-flow, heat-transfer, chemical-reaction in three-dimensional form under transient conditions. By using CFD techniques, the stack model deals more effectively with the complex gas-flow transport processes and the closely inter-related processes than that in the cell mode [4] or in the stack model [5].

This paper presents a continuation of the work on the three-dimensional simulation of an MCFC under steady-state conditions [13]. The study focuses on the modeling of an MCFC stack without internal reforming. The reforming process is studied separately in a reformer model [14]. Throughout the paper, the terms 'fuel cell' and 'stack' refer to the MCFC and the MCFC stack without internal reforming. In addition, the transient conditions are confined to load-following conditions.

2. Stack description

To provide adequate voltage, a fuel cell stack module successively piles up single cells connected in series by separator plates (if there is current collector, this is lumped with the corresponding separator plate in this study). The electricity and heat are generated in the active portion of a cell which consists of electrolyte, anode and cathode. A stack normally operates at a temperature range of 550°C to 750°C and pressure range of 0.1 MPa (ambient atmosphere pressure) to 1 MPa. In practice, a 250 kW fuel cell stack with auxiliaries is contained in a pressure vessel approximately 10.2 m high and 3.6 m in diameter [15].

The fuel and oxidant gases are fed into the stack separately via the anode and cathode input gas manifolds and then they are distributed to each cell where electrochemical reactions take place. The gas-transport in each cell involves the diffusion of the reactant and product gases through the porous electrodes and their flow along cell channels. Finally, the exhaust gases from each cell are discharged through the gas output manifolds. Since the cell electrodes are very good conductors, the voltage of each electrode must be the same everywhere within the cell. The stack output voltage V_{stack} is the sum of each cell voltage $V_{\text{cell}}(k)$. Considering the cells in stack are connected electrically in series, the same current must flow through each cell. The stack output current I_{stack} is the same as each cell $I_{\text{cell}}(k)$, that is:

$$V_{\text{stack}} = \sum_{k=1}^{N} V_{\text{cell}}(k) \tag{1}$$

$$I_{\text{stack}} = I_{\text{cell}}(k)\{k = 1, \ldots, N\} = \int\int i \, \mathrm{d}x \, \mathrm{d}y. \tag{2}$$

3. Main processes

3.1. Stack representation

The stack processes significant to load-following characteristics are the gas transport, chemical reactions, electrical power generation, and heat transfer. Fig. 1 shows the stack structure represented by a series of repeated cells, stack walls and gas manifolds. Each cell contains a cell unit (including electrolyte, anode and cathode), two half-separators, a layer of fuel gas and a layer of oxidant gas. As the stack modeling is at macro-level, the impacts of the processes within the cell unit are represented by the ab-

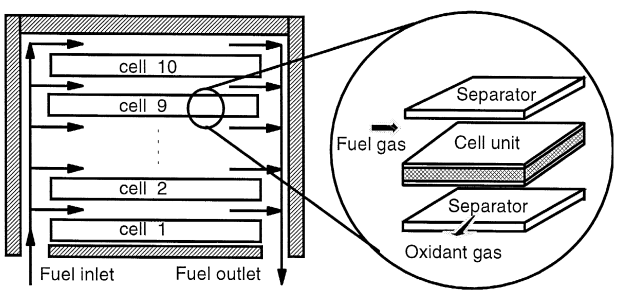

Fig. 1. Representation of a fuel cell stack.

sorption of reactants and the liberation of products at cell unit surface, and by the heat generations within the cell units.

The stack is assumed to have the specifications as follows: (a) the stack has internal gas manifold with cross-flow. The inputs and outlets of the fuel and oxidant gases are located at the bottom of the stack. (b) The fuel and oxidant gases flow in narrow, smooth-walled channels of constant cross-section. (c) The stack wall is completely insulated. However, capabilities to consider the heat transfer between the stack walls and ambient atmospheric gas, or to use stack walls of fixed temperature or fixed heat flux have been built into the model.

In addition, the concentration of the fuel or oxidant gases $\bar{y}$ for gas species of: H_2, CH_4, N_2, CO, CO_2, O_2 and H_2O.

3.2. Gas-transport processes

The gas-transport processes in a stack consists of: (i) the fuel and oxidant gases separately flow through the gas manifolds in the stack direction, where there are no electrochemical reactions, (ii) the fuel and oxidant gases flow along cell channels while there are absorption of the reactants and the liberation of products at cell unit surface, and (iii) the exhaust gases from each cell are discharged through the gas output manifolds.

3.3. Chemical reactions

At the fuel cell electrodes, there are electrochemical reactions as follows:
At the anode:

$$H_2(g) + CO_3^{2-}(l) \Rightarrow H_2O(g) + CO_2(g) + 2e^- \quad (3)$$

At the cathode:

$$\frac{1}{2}O_2(g) + CO_2(l) + 2e^- \Rightarrow CO_3^{2-}(l) \quad (4)$$

The overall cell reaction:

$$H_2(g) + \frac{1}{2}O_2(g) + CO_{2(C)}(g) \Rightarrow H_2O(g) + CO_{2(A)}(g) \quad (\Delta H^\circ_{298} = -242\,\mathrm{kJ/mol}) \quad (5)$$

The impacts of the electrochemical reactions, Eqs. (3) and (4), are represented by the absorption of reactants and liberation of products at cell unit surfaces.

$$\vec{m} = (m_{H_2}, m_{CH_4}, m_{N_2}, m_{CO}\, m_{CO_2}, m_{O_2}, m_{H_2O}) \quad (6)$$

$$\vec{m} = \vec{n} \times \frac{i}{2F} \quad (7)$$

For the electrochemical reaction at anode Eq. (3), $\vec{n}$ is:

$$\vec{n}_{\mathrm{anode}} = (-1,0,0,0,1,0,1). \quad (8)$$

For the electrochemical reaction at cathode Eq. (4), $\vec{n}$ is:

$$\vec{n}_{\mathrm{cathode}} = \left(0,0,0,0,-1,-\frac{1}{2},1\right) \quad (9)$$

In the fuel gas, the water-shift reaction takes place:

$$CO(g) + H_2O(g) \Leftrightarrow CO_2(g) + H_2(g) \quad (\Delta H^\circ_{298} = -41\,\mathrm{kJ/mol}) \quad (10)$$

The water-shift reaction has high reaction speed under high operating temperature (600 ~ 700°C). This reaction rate $\Delta n_{\mathrm{shift}}$ is determined based on equilibrium.

3.4. Electric power generation

The cell-unit performance of the electric power generation is expressed:

$$V = E - \Delta V_{\mathrm{ohmic}} - \Delta V_A - \Delta V_C \quad (11)$$

E is given by the Nernst potential:

$$E = E^\circ + \frac{RT}{2F}\ln\frac{Y_{H_2} \times y_{O_2}^{0.5} \times y_{CO_2(C)}}{y_{H_2O} \times y_{CO_2(A)}} + \frac{RT}{4F}\ln P \quad (12)$$

Sampathe et al. [2], Wolf and Wilemski [1] and Watanabe et al. [4] predicted the local dependence of current density on electrode structure and local operational conditions (e.g., temperature, pressure and gas composition). Our stack model uses the approach of Watanabe et al. [4]. The approach uses the lumped resistance R_{local} to represent the ohmic, anode and cathode resistances. The Eq. (11) is then expressed by Eq. (13).

$$V = E - i \times R_{\mathrm{local}} \quad (13)$$

R_{local} is determined by the cell inherent characteristics and operational conditions (e.g., operating temperature and the gas partial pressure). The formulation of R_{local} is given by Appendix A.

In Eq. (13), the gas concentrations are the values at the anode and cathode surfaces, the temperature is the average cell unit temperature in the stack direction, and gas pressure is either fuel or oxidant gas pressure (as the pressure difference between fuel and oxidant gases is small). The approximation of using average cell-unit temperature is justified because the temperature gradient per cell unit in the stack direction is only a few degrees Kelvin [1]. Consequently, the Nernst potential E in each cell will be in two-dimensional form and independent of stack direction, although different cells may have different performances. Similarly, local current density i, lumped resistance R_{local} will also be in two-dimensional form in each cell.

3.5. Heat transfer

Heat generation occurs in the cell unit in association with electrochemical reactions and cell losses, and there is

heat consumption in the fuel gas due to the water-shift reaction.

The heat generation is assumed to be homogenous in the stack direction in the cell unit, the volumetric heat generation sources q_e (kJ/m^3 s) reads:

$$q_e = \frac{-\Delta H_e \times \frac{i}{2F} - V \times i}{t_{cell}} \quad (14)$$

When the inhomogeneous heat generation in the stack direction is considered, the heat generation in the stack direction is then divided into several zones and the heat generation for each zone is defined. For example, the heat generation from the anode, electrodes and electrolyte, and cathode can be defined separately.

The heat generation q_s (kJ/m^3 s) due to the water-shift reaction is:

$$q_s = \Delta H_s \times \Delta n_{CO} \quad (15)$$

The heat transfer processes include: (i) convective heat transfer between the separators and the gas streams, and between the gas streams and the cell unit, (ii) radiative heat transfer between the separator and cell unit, (iii) conductive heat transfer within the separator, cell unit, and gases, respectively, (iv) energy exchange associated with gas transfer between the gas streams, and (v) conductive heat transfer between adjacent cells in a stack.

4. Stack model

4.1. General consideration

The geometry of stack is divided into three computational regions: input and output gas manifolds and the repeated cells. The processes in the gas manifolds are relatively simple because there are no reactions involved. In addition, the gas flow in the manifold channels is in laminar form, because the gas flow at low speed (smaller than 1 m/s) and the small cross-section of the gas manifold results in low Reynolds number. This section focuses on the establishment of equations for the analysis unit which consists of two half separators, fuel gas, oxidant gas and cell unit (include anode and cathode electrodes and electrolyte). The analysis unit may be repeated partially in either the *x*-, *y*- or *z*-directions to build a stack.

The variables to be solved are the gas velocity in the *x*, *y* and *z* directions, the gas concentration, pressure and temperature, and also the temperature distribution of the cell unit. The stack boundary conditions include the input and output gas streams, the heat transfer between the stack wall and the surroundings, and also the required current density. With regard to the processes described in Section 3.4, the main processes modeled for the analysis unit are: (i) gas-transport of fuel and oxidant, (ii) water-shift reaction in the fuel gas, (iii) absorption of reactants and liberation of products at cell unit surfaces due to electrochemical reactions, (iv) heat generation in cell unit due to the electrochemical reactions and cell losses, and (v) heat transfers among the separators, gas and cell unit, and the heat conduction in separators and in cell unit. The modeling equations comprise: (i) a set of conservation equations of gas species, energy and momentum, (ii) the auxiliary equations to compute the terms in the conservation equations, and (iii) boundary conditions.

It is assumed that the flows of the fuel and oxidant gases in the channels are laminar in form. This assumption is based on the low gas speed and small dimension of the gas channel. It is also assumed that the fuel and oxidant gases are Newtonian fluids.

4.2. Conservation laws

4.2.1. Conservation of a chemical species

The conservation of m_l is expressed as

$$\frac{\partial}{\partial t}(\rho m_l) + \mathrm{div}\left(\rho \vec{V}_{m_l}\right) = R_l \quad (16)$$

Here $\partial(\rho m_l)/\partial t$ denotes the rate of change of the mass of the chemical species per unit volume. The quantity $\rho u m_l$ is the convection flux of the species. The quantity R_l on the right-hand side is the rate of generation of the chemical species per unit volume. For the fuel gas, R_l is the rate of the water-shift reaction multiplying the stoichiometric number of the gas species. For the oxidant gas, there is no reaction, R_l is zero.

4.2.2. Conservation of energy

The energy equation for fuel and oxidant gases can be written as

$$\frac{\partial(\rho h)}{\partial t} + \mathrm{div}\left(\rho \vec{V} h - \frac{\lambda \nabla h}{C_p}\right) = S_h \quad (17)$$

For the fuel gas, S_h is heat generated by the water-shift reaction q_s (Eq. (15)). For the oxidant gas, there is no heat source, S_h is zero.

The energy equation for the separator and cell unit can be written as

$$\rho C_p \frac{\partial(\rho T)}{\partial t} - \vec{\lambda} \times \nabla^2 T = S_h \quad (18)$$

for the separator, there is no heat generation, S_h is zero. For the cell unit, the heat generation S_h is the q_e (Eq. (15)).

4.2.3. Momentum balance

The differential equation governing the conservation of momentum for the fuel gas in a given direction for a

Newtonian fluid and laminar flow, which are assumed, can be written as.

$$\frac{\partial(\rho u)}{\partial t} + \mathrm{div}\left(\rho \vec{V} u - \mu \nabla u\right) = -\frac{\partial p}{\partial x} + B_x + V_x \qquad (19)$$

where B_x is the x-direction body force pure unit volume, and V_x stands for the viscous terms that are in addition to those expressed by div($\mu \nabla u$).For the oxidant gas:

$$\frac{\partial(\rho w)}{\partial t} + \mathrm{div}\left(\rho(\vec{V}) w - \mu \nabla w\right) = -\frac{\partial p}{\partial z} + B_z + V_z \qquad (20)$$

4.2.4. A general equation

Due to the similarity in forms of the above conservation equations, we can write Eqs. (16)–(20) as a general equation:

$$\frac{\partial}{\partial t}(\rho\phi) + \mathrm{div}\left(\rho \vec{V}\phi - \Gamma_{\phi,\mathrm{eff}} \nabla\phi\right) = S_\phi \qquad (21)$$

where $\vec{V}$ is the velocity vector, ϕ stands for any one of the dependent quantities: gas species (C), energy (h), momentum (u) and continuity 1, $\Gamma_{\phi,\mathrm{eff}}$ is the effective exchange coefficient, and S_ϕ is the source or sink term.

5. Computational fluid dynamic approach

Since there is not an exact mathematical solution for Eq. (21), computational fluid dynamic (CFD) methods, have to be introduced to get the discrete solution. Details of various numerical schemes were given by Patankar [16].

The implementation of the stack model uses a CFD program PHOENICS [12]. The stack CFD code involves: (i) definition of an appropriate computational grid, and (ii) description of the stack-inherent characteristics (e.g., stack geometry and physical properties) and the operational conditions. This section demonstrates the establishment of the grid by defining the grid cells for a single cell and using appropriate time steps for the simulations under transient conditions. The stack-inherent characteristics are provided by He [17] and the stack operation conditions are given in Appendix B.

The stack grid is comprised of that for stack walls, gas manifolds and a series of repeated cells. Fig. 2 illustrates the grid definition for an analysis unit of 20 mm × 20 mm. A cell unit with dimensions of 1 m × 1 m will consists of 50 × 50 such a basic unit. The x, y and z axes represent the fuel gas channel direction, the stack direction, and oxidant gas direction, respectively. The cell height (in the y direction) is scaled up for the illustration and it has five zones: two for half-separators and three for fuel gas, cell unit, and oxidant gas. The grid definition is based on the requirement of the minimum grids. The minimum grids are one for each of the two half-separators, three for the cell unit (two electrodes and electrolyte), five for fuel gas and five for oxidant gas (parabolic gas velocity). The minimum grids in x- and z-directions are not straightforward. The grid in the x direction is denser than that in the z direction because the variation in the fuel gas composition is more significant than that of oxidant gas (the designed fuel gas

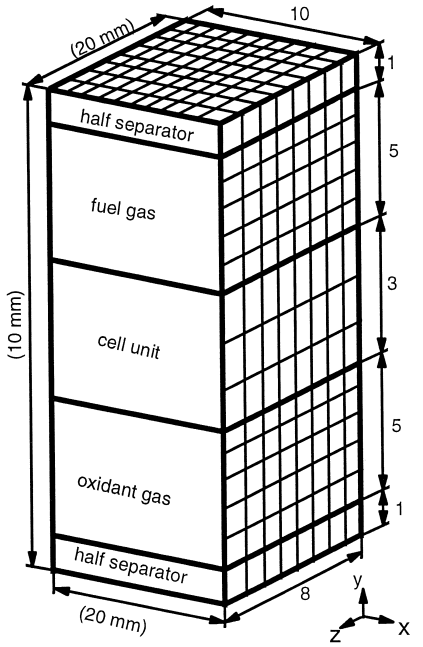

Fig. 2. Dimensions and computational grids for an analysis unit.

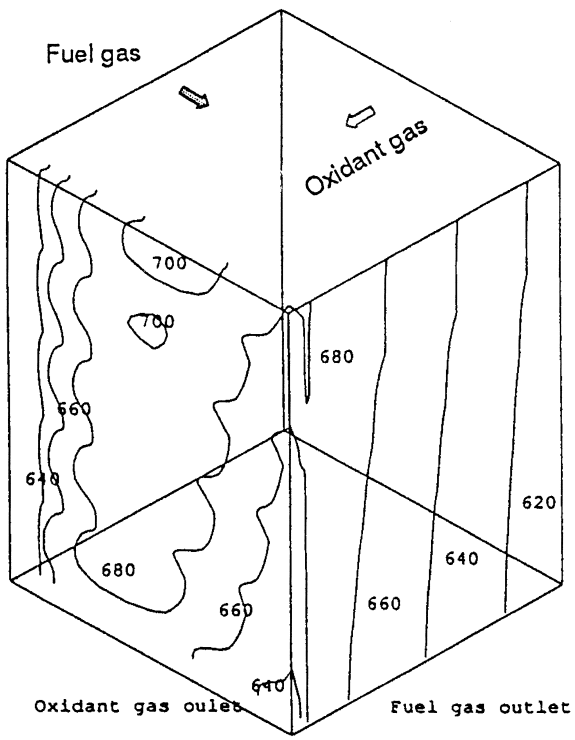

Fig. 3. Initial stack temperature profile.

utilization is higher than that of oxidant gas). The grids eight and ten have been used for *x*- and *z*-directions, and appear feasible.

As the simulation is conducted under transient conditions, fine time steps are needed for a step or ramp change. For example, a +10% step change in voltage is simulated by a 100 step changes of +0.1% voltage in 0.1 s.

Several parameters of PHOENICS program are often manipulated during the simulations. For example, the selection of a time step has an important impact on both the simulation time and the accuracy and it is crucial to a successful simulation. A denser time step usually results in easier convergence in each step because smaller variations of parameters occur in each step.

In transient conditions, the simulation results at one time step serve as the initial conditions for the next time step. Consequently, the computational errors of each time-step grid may be accumulated. However, no general rules

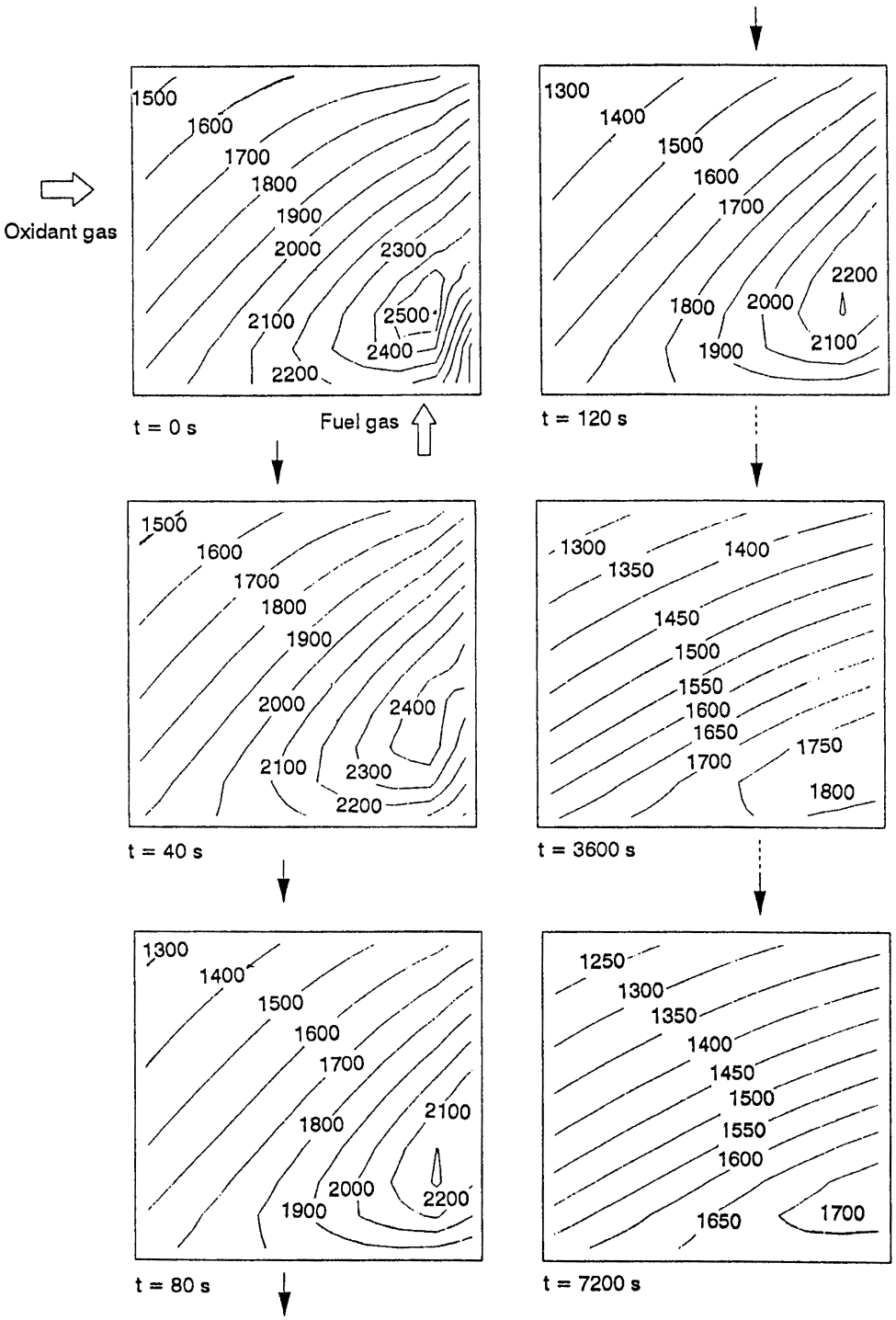

Fig. 4. Current density profile response at a transverse section (A/m^2).

are available to evaluate the simulation results. We use the procedure of first conducting an additional steady-state simulation under the final state of the transient condition, and then comparing the results of the transient simulation over a long time with those of the steady-state simulation. If the transient simulation results over a long time are in agreement with those for the steady-state simulation, the transient results are considered to be acceptable.

6. Case setup

To evaluate the above described stack model, the responses of current density and temperature distributions are illustrated for a +10% step change of stack voltage. The stack voltage or current output can be simultaneously manipulated to accommodate small load variations. However, when there are large variations in load, the flow-rates

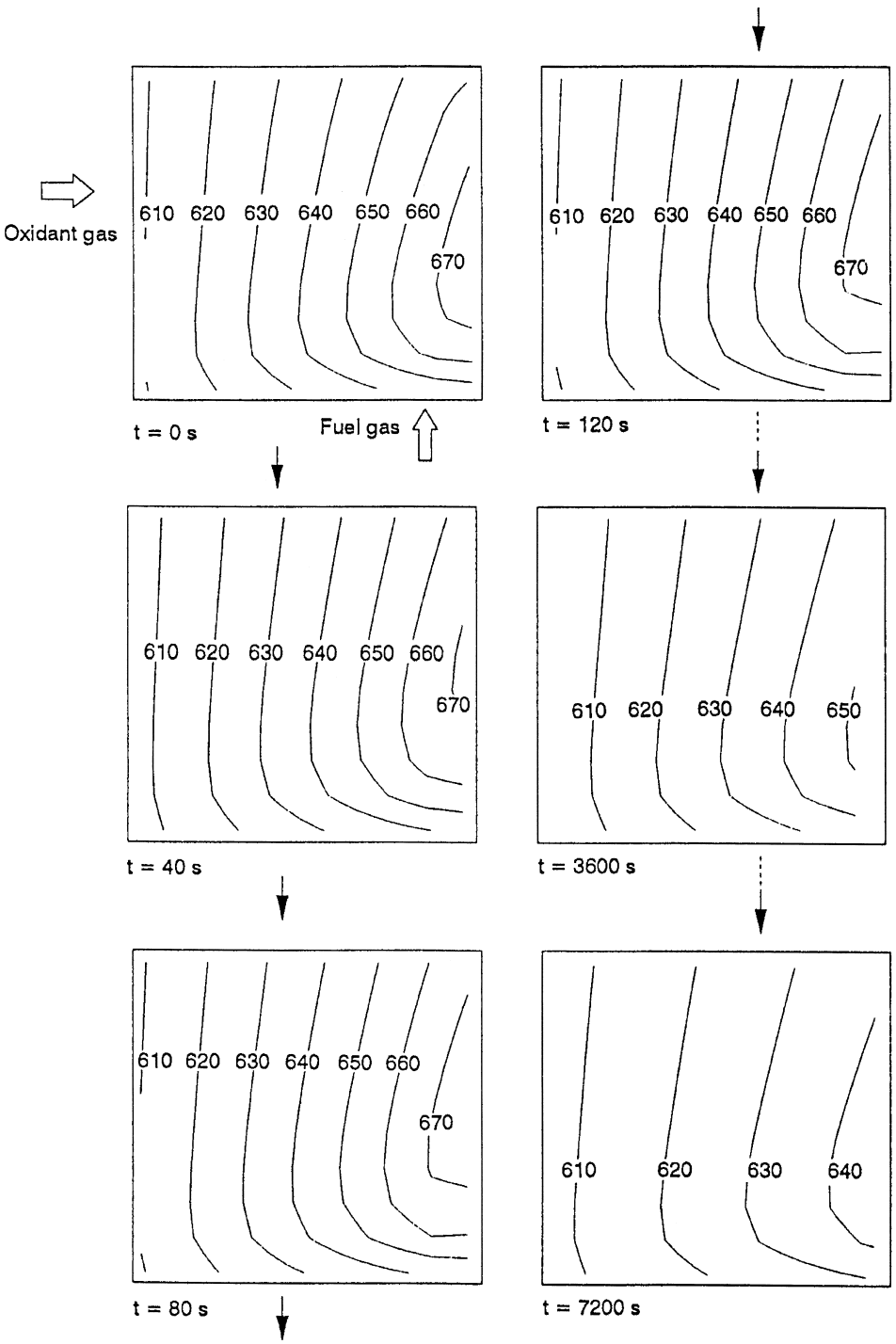

Fig. 5. Temperature profile response at a transverse section (°C).

of fuel and oxidant gases stack may also be changed to maintain the stack fuel and oxidant utilizations within the allowable ranges. The change of gas flow rates is often slower than that of voltage or current. This case setup represents one of the severe operating conditions for a stack under load-following modes.

The inlet temperature of both fuel and oxidant gas is 600°C, and the stack operation pressure is 0.3 MPa. The initial stack voltage operates at 3.5 V (cell voltage is around 0.7 V), and the flow-rates of fuel and oxidant are 0.23 mol/s and 3.82 mol/s, respectively [17].

7. Results and discussion

The time needed for a stack current or temperature to reach a new steady-state is about 1 or 2 h [11]. The simulation for the stack response is for a period of 2 h. A smaller time-step is used at the beginning and is increased progressively. The simulation results are illustrated for $t = 40$, 80, 120, 3600 and 7200 s, respectively.

Fig. 3 shows the stack temperature profile under the initial conditions. The results are used to identify the maximum temperature and gradient locations. In this case, the maximum temperature is in the top cell near the oxidant gas outlet.

Fig. 4 illustrates the current density distribution in the separator of cell unit five. Between 0 s and 80 s, the current density profile changes significantly, but not between 80 s and 120 s. The current density profile continues to change between 120 s and 3600 s, and also between 3600 s and 7200 s. The magnitude of current density changes rapidly in the beginning and slowly in the following stage. For example, the maximum current density decreases by 300 A/m^2 (from 2500 to 2200 A/m^2) between 0 s and 80 s, but decreases only by 100 A/m^2 (from 1800 to 1700 A/m^2) between 3600 s and 7200 s. This indicates that the current has fast change due to the variation of voltage and gas concentration, after which the current has a long term decrease due to the variation of cell potential and losses caused by the temperature decrease.

Fig. 5 shows the dynamic temperature distribution in the middle layer of the separator for cell unit five. The temperature profile changes slowly. For example, the maximum temperature remains 670°C between 0 s and 120 s, decreases by 20°C after 1 h and by another 10°C after a further hour. The overall temperature decreases with time, which agrees with Eq. (10) that higher stack voltage provides smaller current density corresponding to less heat generation.

Comparison of the changes of the current and temperature distributions in Figs. 4 and 5 indicates the relationship between the current and temperature. Between $t = 80$ s and 120 s, the current profile in Fig. 4 remains almost the same, which agrees with the constant temperature profile in Fig. 5. Due to the variation in temperature, the current density profile then continues to change between 120 s and 3600 s and also between 3600 s and 7200 s. The results given in Figs. 4 and 5 also confirm that the current density and temperature distributions are within the safety constraints with regard to the allowed maximum temperature and temperature gradients [17] under a +10% step voltage change.

8. Model evaluation

Many assumptions and approximations have been made to achieve this stack model. The stack model therefore requires experimental validation. Usually, the temperatures

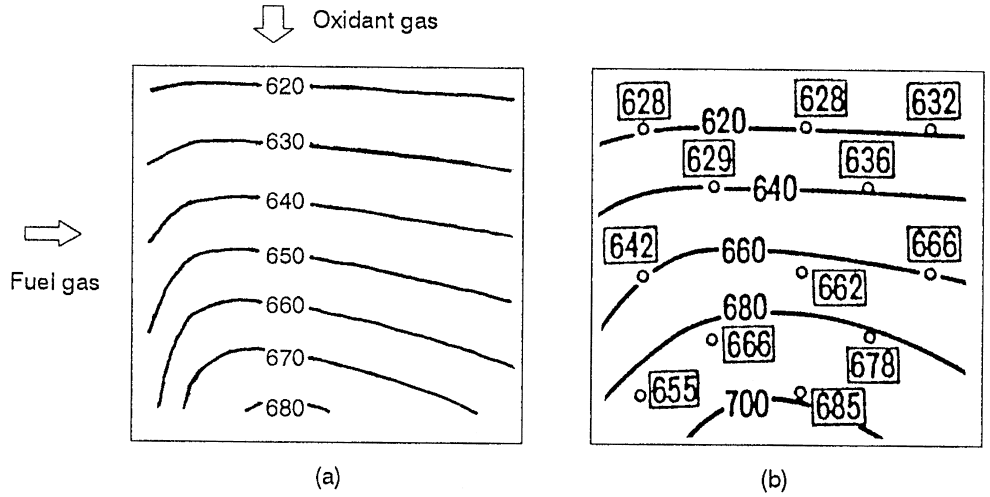

Fig. 6. Comparison of temperature distributions (a) the computed results with the model, and (b) analytical profiles and measured data (°C).

at various locations can be measured under steady-state conditions, and measurement under transient conditions may have difficulties [18]. Even under steady-state conditions, the measurement of the current density distribution is not easy, but it may be approached by measuring the gas concentrations at various locations.

The model performance under steady-state conditions is evaluated by a comparison between the temperature profiles from our model and the analytical and measured temperature distributions described by Fujimura et al. [5]. The system for measuring the cell temperature distribution was described by Kobayashi et al. [18]. Our model has been applied to calculate the measured stack which had 10 cells with cell dimensions of 0.36 m^2 [18].

Fig. 6a is the computed temperature distribution of the middle layer of oxidant gas in the middle cell and Fig. 6b gives the simulated (continuous lines) and the measured (discrete dots) temperature distributions. The profiles of the computed temperature from our model are similar to the simulated profiles. Since few measured data are available, drawing the isotherm lines based on these data is not feasible. The predicted temperature profiles agree reasonably with the simulated results, and the deviations between the computed isothermal lines and most of the measured data are less than 10°C. Therefore, the performance of our model is acceptable. The model validations under both steady-state and transient conditions will be continued. For example, it has been suggested that the validation of the current density profile may be achieved by measuring the gas concentration at various locations under steady-state and transient conditions.

9. Conclusions

An exploration of the parameters distribution in an MCFC stack under transient conditions using dynamic simulations has been presented. The stack model implemented in CFD program represents the processes of gas transport, chemical reaction and heat transfer at cell level, and the heat and gas transport at stack level, and incorporates the electrode power generation characteristics. The simulation-derived current and temperature distributions under a step voltage change have shown that the current density profile changes rapidly in the beginning and slowly in the following stage and that the temperature response is slow. The simulation results have indicated the usefulness of the model in evaluating the safe and efficient operation of the stack under transient conditions, and have also showed that the stack implementation using CFD is a promising approach. Although the model prediction of the temperature profiles agrees reasonably with the simulated results from the literature, and the deviations between the computed isothermal lines and most of the measured data are acceptable, further validation of the stack model is necessary.

10. List of symbols

A_R	frequent factor of the resistance
C_p	heat capacity (kJ/kg)
E	reversible potential of the cell (V)
E°	reversible potential of the cell (V)
F	Faraday constant (96,485 C/mol)
h	gas enthalpy (kJ/mol)
ΔH°_{298}	standard heat available from reaction (kJ/mol)
ΔH_e	enthalpy change of the overall cell electrochemical reaction (kJ/mol)
ΔH_s	enthalpy change of the shift reaction (kJ/mol)
ΔH_R, ΔH_A and ΔH_C	activation energy of internal resistance, anode and cathode (J/mol K)
i	local current density (A/m^2)
I	total current output (A)
k	cell number
m_l	mass fraction of a chemical species l (mol/s)
$\vec{m}$	gas absorption or liberation flow rate from electrode surface (mol/m^2 s)
Δn_{CO}	rate of the shift reaction (mol/m^3 s)
$\vec{n}$	reaction stoichiometric number of gas species: H_2, CH_4, N_2, CO, CO_2, O_2 and H_2O
N	total cell number
P, p	gas operation pressure (10^5 Pa)
R_{oA} and R_{oC}	anode and cathode resistances
R	gas constant
R_{local}	lumped local resistance (Ω)
S_h	volumetric rate of heat generation (kJ/m^3 s)
S_ϕ	general source or sink term
t	thickness (m)
T	temperature (K)
u, v, w	velocity magnitude in x, y, and z direction (m/s)
$\vec{V}$	gas velocity vector (m/s)
V	voltage (V)
ΔV_{ohmic}, ΔV_A and ΔV_C	voltage losses due to ohmic and overpotential at electrodes
x, y and z	cell length, width and height (m)
y	gas molar fraction

Greek letters

λ	thermal conductivity (W/m K)
μ	viscosity
ρ	molar density (kg/m^3)

Subscripts

A	anode side
C	cathode side
cell	cell level
stack	stack level

Abbreviations

g	gas
m	melt
CFD	computational fluid dynamics
MCFC	molten carbonate fuel cell
PAFC	phosphoric acid fuel cell
PEM	proton exchange membrane
SOFC	solid oxide fuel cell

Acknowledgements

The first author wishes to thank Professors R.W.J. Kouffeld and O.H. Bosgra for the opportunity to perform the investigation. We acknowledge the useful suggestions by Mr A. Korving, Dr J.G.M. Becht, Dr S. Dijkstra and V. Lorraine van Dam.

Appendix A. Calculation of the lumped resistance

Our stack model uses the empirical equation proposed by Watanabe et al. [4] to calculate the lumped resistance. The lumped resistance R_{local} in Eq. (13) is comprised of ohmic, anode and cathode resistances and reads:

$$R_{\text{local}} = A_{\text{R}}\exp\left(\frac{-\Delta H_{\text{R}}}{RT}\right) + \exp\left(\frac{-\Delta H_{\text{A}}}{RT}\right) \times \ln\left(R_{\text{oA}} P_{\text{H}_2}^{a} P_{\text{CO}_2\text{A}}^{b} P_{\text{H}_2\text{OA}}^{c}\right) + \exp\left(\frac{-\Delta H_{\text{C}}}{R}\right) \ln\left(R_{\text{oC}} P_{\text{O}_2\text{C}}^{d} P_{\text{CO}_2\text{C}}^{e}\right) \qquad \text{(A.1)}$$

where P_{i} is partial gas pressure of a species i. Superscripts from a to e are coefficients which are related to the cell inherent performance. These coefficients are identified from the experimental data. Therefore, the lumped resistance R_{local} depends on the electrode inherent characteristics and operational conditions (e.g., the temperature and the gas partial pressures).

Appendix B. Description of the stack operational conditions

The stack operational conditions in PHOENICS code include the variables to be solved, the initialization, and the boundary and source conditions. These are as follows: (a) the variables to be solved in the conservational equations are the gas velocity in the x, y and z directions, the gas composition and pressure, and also the temperature in the repeated cells (including gas, separator and cell unit), in the stack walls, and in the gas manifolds. (b) Initialization of the above variables to be solved. (c) The boundary conditions include the input and output gas streams, the heat transfer between the stack wall and the surroundings, and also the required current density. The defined boundary conditions are the gas velocity in the x, y and z directions, the gas composition and temperature at inlet gas streams, and the gas pressure at outlet gas streams. The impacts of the cell unit are represented by the absorption of reactants and the liberation of products at cell unit surfaces, and by the heat generation due to the electrochemical reactions and cell losses in volumetric heat sources within the cell unit. The absorption of reactants and the liberation of products at cell unit surfaces are expressed by Eq. (7), and the volumetric heat source within the cell unit is expressed by Eq. (14). The heat generation (or consumption) in the fuel gas due to water-shift reaction is also represented in volumetric heat sources, and expressed by Eq. (15).

As the stack inherent characteristics (e.g., stack geometry and physical properties) and the operational conditions have been represented in the stack code, the CFD program calculates the local characteristics. For example, the heat transfer coefficient was computed according to the physical properties of the gas and solid, the gas velocity and temperature [12]. In addition, several sub-routines have been developed for calculating the nonstandard local characteristics, such as the chemical reaction rates, the power generation in cell unit, and the properties of gas streams [17].

References

[1] T.L. Wolf, G.J. Wilemski, J. Electrochem. Soc. 130 (1) (1983) 48–55.
[2] V. Sampathe, A.F. Sammells, J.R. Selman, J. Electrochem. Soc. 127 (1980) 79.
[3] G.K. Wilemski, A. Gelb, Molten Carbonate Fuel Cell Performance Model Update: Final Report, Physical Sciences, Research Park, Andover, MA, USA, 1985.
[4] T. Watanabe, E. Koda, et al., Development of Molten Carbonate Fuel Cell Stack Performance Analysis Model, Yokosuka Research Laboratory, Rep. No. W90028, Japan, 1991, 30 pp. (in Japanese).
[5] H. Fujimura, N. Kobayashi, K. Ohtsuka, Heat and mass transfer in a molten carbonate fuel cell (performance and temperature distribution in a cell stack), JSME Int. J. Jpn. Ser. II 35 (1) (1992) 81–88.
[6] T. Shinoki, M. Matdumura, A. Sasaki, Development of an internal reforming molten carbonate fuel cell stack, IEEE Trans. Energy Conver. 10 (4) (1995) 722–728.
[7] M. Yamaguchi et al., Analysis of control characteristics using fuel cell plant simulator, IEEE Trans. Ind. Electron. 37 (5) (1990) 378–386.
[8] T. Kivisaari, Aspen Plus studies of MCFC co-generation systems,

presented at Fuel Cell Seminar, November 29–December 2, Tucson, AZ, USA, 1992, pp. 325–328.
[9] A. de Groot, N. Woudstra, Energy analysis of a fuel–cell system, J. Inst. Energy 68 (1995) 32–39.
[10] E.E. Achenbach, Three-dimensional and time-dependent simulation of a planar solid oxide fuel cell stack, J. Power Sources 49 (1994) 333–348.
[11] E.E. Achenbach, Response of a solid oxide fuel cell to load change, J. Power Sources 57 (1995) 105–109.
[12] CHAM, The PHOENICS Reference Manual, TR200, CHAM, London, 1995.
[13] W. He, Q. Chen, J. Power Sources 55 (1995) 25–32.
[14] W. He, Modeling a Reformer in Fuel Cell Power-Generation Systems, ASME, Heat transfer and fluids engineering divisions, HTD-Vol. 321, FED-Vol. 233, The American Society of Mechanical Engineers, USA, 1995, pp. 317–325.
[15] T. Kahara, M. Kunkata, et al., Status of MCFC Stack Technology Development at Hitachi, The 2nd International Fuel Cell Conference, February 5–8, Japan, 1996, pp. 123–126.
[16] S.V. Patankar, Numerical Heat Transfer and Fluid Flow, McGraw-Hill, New York, 1980.
[17] W. He, Solution Techniques for a Molten Carbonate Fuel Cell Stack Using PHOENICS Program, Internal report, Delft University of Technology, Delft, The Netherlands, 1997, 100 pp.
[18] N. Kobayashi, H. Fujimura, K.K. Ohtsuka, Heat and mass transfer in a molten carbonate fuel cell (experimental and analytical investigation of fuel cell temperature distribution), JSME Int. J. Jpn. Ser. II 32 (3) (1989) 420–427.